

# **PIC simulation of particle behavior in an Inertial Electrostatic Confinement Fusion device using XOOPICTM code**

**D. Bhattacharjee<sup>1</sup>, S. Adhikari<sup>2</sup>, N. Buzarbaruah<sup>1</sup> and S. R. Mohanty<sup>1,3</sup>**

<sup>1</sup> Center of Plasma Physics-Institute for Plasma Research, Sonapur, Kamrup, Assam, 782402, India

<sup>2</sup>Department of Physics, University of Oslo, PO Box 1048 Blindern, NO-0316 Oslo, Norway

<sup>3</sup> Homi Bhabha National Institute, Anushaktinagar, Mumbai, Maharashtra, 400094, India

E-mail: smruti@cppipr.res.in

**Abstract.** The kinetic analyses are quite important when it comes to understand the particle behavior in any device as they start to deviate from continuum nature. In the present study, kinetic simulations are performed using Particle-in-Cell (PIC) method to analyze the behavior of ions inside a cylindrical Inertial Electrostatic Confinement Fusion (IECF) device which is being developed as a tabletop neutron source. Here, the lighter ions, like deuterium are accelerated by applying an electrostatic field between the chamber wall (anode) and the cathode (cylindrical gridded wire), placed at the center of the device. These ions recirculate across the cathode grid, which in turn capable of producing fusion reaction at the central region of the device. An open source PIC code (XOOPICTM) is used in our study to simulate the ion dynamics at different experimental conditions. The plasma potential profiles obtained from the simulated results indicate the formation of multiple potential well structures inside the cathode grid depending upon the applied cathode potential (from  $-1$  to  $-5$  kV). The ion density at the core region of the device is found to be of the order of  $10^{16} \text{ m}^{-3}$ , which closely resembles the experimental observations. Spatial variation of Ion Energy Distribution Function (IEDF) has been measured in order to observe the characteristics of ions at different cathode voltages. Finally, the simulated results are compared and found to be in good agreement with the experimental profiles. The present analysis can serve as a reference guide to optimize the technological parameters of the discharge process in IECF devices.

## 1. Introduction

An inertial electrostatic confinement fusion (IECF) device operates on the principle of the confinement of plasma particles in a purely electrostatic field. In this device, ions are recirculated across the gridded cathode, confined and remain inside the system unless they collide with the neutrals, background ions and cathode grid wires. As a result, the secondary electron concentration also increases near the core region. The electrostatic potential produced by both the ions and electrons plays a vital role behind the fusion process in the system. The secondary electrons neutralize the space charge of ions and thus maintain the ion recirculation across the gridded cathode [1]. The highly energetic ions fused together at the core region and produce particles like neutron, proton etc. Unlike magnetic and laser-based confinement methods, which are primarily effective for long term power production, the IECF concept is being developed for the near term applications [1, 2]. The theoretical concept of IECF was first proposed by P. Farnsworth [3], and later, it was studied experimentally by R. Hirsch [4] in 1970's. Different types of IECF devices have been developed till date, e.g., Hirsch [4] introduced ion-gun injectors to confine ions, Nebel *et al.* [5] used a triple grid design for better confinement of the ions. Bussard [6] developed a magnetic-electrostatic version and other researchers came up with new versions such as single-grid [7], multiple-grid [8, 9] magnetron assisted device etc. The potential profiles in the IECF device were first experimentally studied by Swanson *et al.* [10] using electron beam probing. Later, Thorson *et al.* [11, 12] used emissive probe for the measurement of potential and ion density profile in the central region of the spherical IECF device by varying the gas pressure. Moreover, Yoshikawa *et al.* [13] have carried out experiments for the direct measurement of potential by using laser-induced fluorescence technique. Over the years, researchers of different laboratories across the world (University of Wisconsin, University of Illinois, Tokyo Institute of Technology, Kyoto University etc.) [14–19] have been continuously devoting their effort for upgrading the IECF device in terms of neutron production as well as its applications. As far as the theoretical studies are concerned, Nevin [20] has presented a model for the ion distribution function and is able to reproduce some of the essential features of the IECF system, like electrostatic confinement, strong ion peak at the center and a nearly mono-energetic distribution of the ions. Krall [21] and Dolan [22] introduced the polywell concept in the spherical IECF device in which potential well structures have been studied in order to achieve maximum fusion rate. The purpose of their work was to establish the IECF scheme as an alternate way to achieve thermonuclear fusion energy. However, later on it was confirmed that the IECF scheme shows little promise as a basis for the development of commercial electrical power plant [20]. Ohnishi *et al.* [23] observed the formation of potential well structure inside the cathode grid depending upon the magnitude of ion current. They have studied the dynamic behaviors of potential well by performing numerical simulations on the basis of particle-in-cell (PIC) method. A correlation between the D-D neutron production rate and the depth of the potential well is also established in their work. Ohnishi *et al.* [24] further improved the PIC code to enhance the computational speed and accuracy. However, they considered only the  $D_2^+$  ions while  $D^+$  ions are not included in the simulation. Again, the angular momentum that

the ions acquire due to coulomb interaction and collision with the neutrals is not considered in the simulation. Buzarbaruah *et al* . [25] tried to track the trajectory of the  $D^+$  ions by performing simulation using Simion code [26]. However, the limitation of the code did not allow to create the plasma environment inside the system, rather it could only provide the electric or magnetic field to observe the possible trajectories of ions.

Since the potential profiles and ion density profiles play an important role for the optimization of the neutron production rate [12] (during higher voltage operations), a detailed study of these profiles during lower cathode voltage conditions become equally important for a complete understanding of the underlying physics of the IECE scheme. In this work, we have studied the behavior of potential well and ion density profiles in the cylindrical IECE [25, 27, 28] device during relatively lower cathode potential (up to  $-5\text{ kV}$ ) using XOPIC code [29] [X11-based Object-Oriented Particle-In-Cell on X-windows, developed at the University of California, Berkley]. The code is capable of producing the exact experimental scenario and all the essential parameters associated with the plasma can be extracted for analysis. Ion energy distribution function (IEDF) is also obtained at various locations of the simulated region for different cathode voltages. The simulated profiles then compared with the experimental to benchmark the results. In the next section, the experimental setup, procedures and the diagnostics used for the experiment are described. In section 3, we briefly describe the simulation parameters and the code used in this simulation. The simulated results such as, potential well profile, ion density profile and the IEDF are described in the section 4. The experimental results and their comparisons with the simulated results are also discussed in the same section. The last section of the paper contains the concluding remarks and the future scopes.

## 2. Experimental setup and procedure

The IECE device used in this study consists of a cylindrical stainless steel vacuum chamber having a diameter of  $50\text{ cm}$  and a height of  $30\text{ cm}$ . A highly transparent cylindrical cathode is kept vertically at the center of the chamber, which acts as the anode (grounded). The cathode that is connected to a high voltage power supply through a feedthrough, consists of tungsten grid wires of varying diameters. In this work, we have used a cathode of diameter  $3\text{ cm}$  ( $\sim 95\%$  transparent), made up of 8 numbers of grid wires having diameter  $0.12\text{ cm}$ , each. Different ports are there in the chamber for evacuation, viewing, coupling high voltage feedthrough, inserting gas and other diagnostic tools. A schematic diagram of the cylindrical IECE device used in the present work is shown in the figure(1). The chamber is evacuated by using a turbo molecular pump backed by a rotary pump and the pressure is maintained inside the chamber by a coarse feed valve.

The deuterium plasma is created by adopting hot cathode discharge (i.e. filamentary discharge) method in which two thoriated tungsten filaments are placed at two diagonally opposite positions and at  $10\text{ cm}$  away from the wall of the chamber. The filaments are heated to produce thermionic electrons and a discharge voltage and current of  $80\text{ V}$  and  $200 - 500\text{ mA}$  is maintained, respectively, at a working pressure of  $\sim 10^{-3}\text{ Torr}$ . Then, negative voltage is

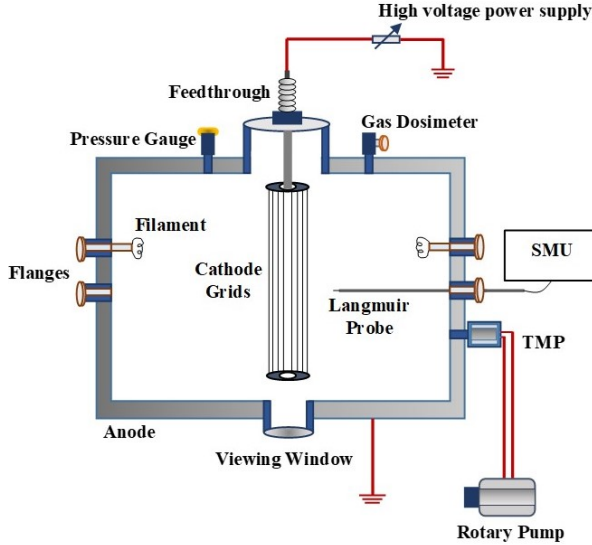


Figure 1: Schematic diagram of the cylindrical IECF device with different accessories.

applied to the cathode through the feedthrough using a 5000 V, 600 mA DC power supply. A cylindrical Langmuir probe of length 0.5 cm and diameter 0.05 cm has been used to characterize the plasma. The probe is inserted into the plasma through one of the ports, as shown in the figure(1), and it is movable radially from the wall of the chamber to the center of the cathode. The potential at different positions inside the chamber is measured from the Langmuir probe. We have varied the applied cathode voltage from  $-1$  to  $-5$  kV in order to observe the modifications in potential profile structure inside the cathode region [30]. In order to measure the plasma temperature and hence the ion density, we have used a double Langmuir probe.

### 3. Modeling

To understand the complex behavior of ions inside the cylindrical IECF device, we have performed electrostatic particle-in-cell (PIC) simulation using XOOPIIC code. XOOPIIC has the capability of handling two-dimensional space in cartesian and cylindrical geometries, including all three velocity components, with in-built electrostatic and electromagnetic models available. The code can deal with an arbitrary number of species and it includes Monte Carlo Collision (MCC) algorithms for modeling collisions of the charged particles with themselves and with the background gas. The important benefit of the XOOPIIC code is that it couples the field solution with the particle mover, whereas most of the other techniques explored has to involve two separate codes for this. The other difficulty is the insertion of non-symmetric geometries into the system. The simulated dimension and parameters are designed to recreate the actual experimental scenario in this paper. The simulation geometry is a horizontal 2D cross-section of the device including the cross-section of the cathode grids, (figure(2)) as per the experimental setup. Since the dimension of the cathode grid wires are very small as compared to the dimension of the simulation domain, we have considered it

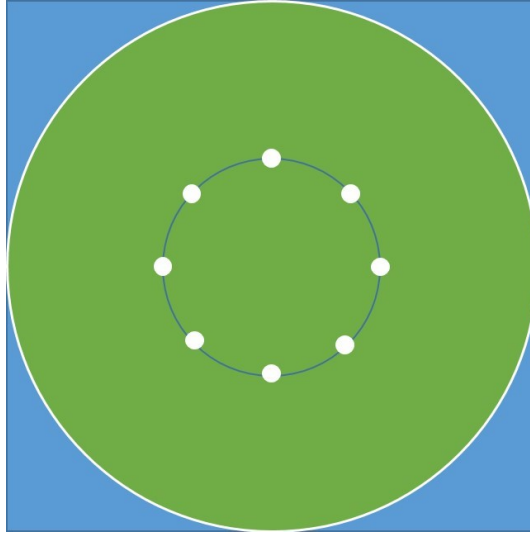


Figure 2: Cross-section of simulation region with the cathode grid.

Table 1: Simulation parameters

Parameters	Values
Grid size	$104 \times 104$
Length	$0.14 \text{ m}$
Width	$0.14 \text{ m}$
Time step (dt)	$10^{-10} \text{ s}$
Specific weight	$10^9$
Background gas	Deuterium
Cathode potential	$-1 \text{ kV}$ to $-5 \text{ kV}$
Anode potential	$0 \text{ V}$

as square shaped rather than circular for simplification of the simulation. We have modeled electron emitters inside the simulation domain, each emitting a constant and equal flux of electrons continuously into the system. The emitted electrons interact with the background gas (deuterium) and produce ionization. A high negative voltage is applied to the cathode grid wires, due to which ions are accelerated towards it. The system is assumed to be bounded and symmetric. The time step for the simulation has been chosen in order to satisfy the Courant condition [31] so that the particles must not fly over more than one cell in one time step. In order to get a good resolution of phase space, it requires an extremely large number of computational particles (super particles). However, considering so it is important to optimize the number as it significantly influences the total run-time. In PIC simulation, the trajectory of every super-particle is computed kinetically. Therefore, longer domain length with a large number of super particles requires much longer run time to solve the problem. Again, the statistical noise associated with PIC simulation also increases with the increase in domain length. To avoid this, a large number of computational particles with relatively shorter domain

length is appropriate for the simulation to obtain the desired results. The code is capable of running in both GUI (Graphical User Interface) and non-GUI modes. To reduce the execution time, the non-GUI mode is generally preferred. A typical computer run takes at least 3 – 4 hours to achieve the steady-state. After reaching the steady-state, the diagnostics are saved as ASCII data files. The simulation parameters used in this work are depicted in the table 1. The primary electron and ion temperatures are assumed to be 3 and 0.1 eV, respectively. A few subroutines have also been developed in MATLAB® to visualize the simulation data.

## 4. Results and Discussions

At first, we have tried to visualize the ion re-circulation from the ion phase space data. The phase space of ion, after attaining the steady-state for  $-1$  kV applied cathode voltage, is shown in figure(3a). It clearly shows the re-circulation of ions across the openings of the cathode grid. Some of the ions are getting trapped inside the cathode and their density is found to be increasing at the central core region. The increase in ion density inside the cathode mainly depends upon the applied cathode voltage. The photograph taken from the bottom of the cylindrical IECF device during  $-1$  kV cold cathode discharge operation [27], as shown in figure(3b), indicates that ion spokes are coming out of the core region of the cathode. This mode of operation is popularly known as the star mode [32] in IECF system. The surface plot of potential and ion density profiles obtained from the XOOPIIC data during  $-1$  kV applied cathode voltage, are shown in figure(4). A detailed discussion of the potential and ion density profiles are done in the next subsection.

### 4.1. Potential and ion density profiles

Voltage ranging from  $-1$  to  $-5$  kV is applied to the gridded cathode to observe the modifications in the potential profiles, specially inside the cathode region. After attaining the steady-state in the simulation, the obtained potential profiles are plotted in the MATLAB scripts for better analyses. The equatorial plots of the potential profiles for different cathode

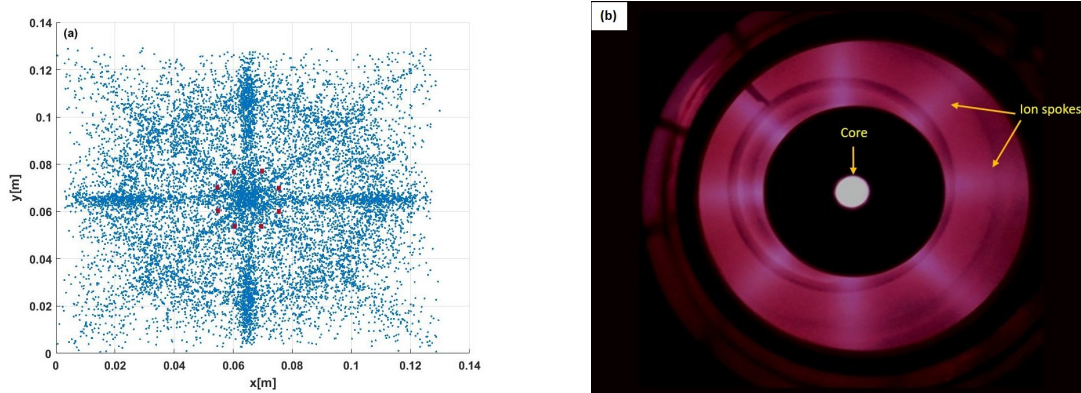


Figure 3: Observation of re-circulation of ions in both simulated profile (a) and experiment (b).

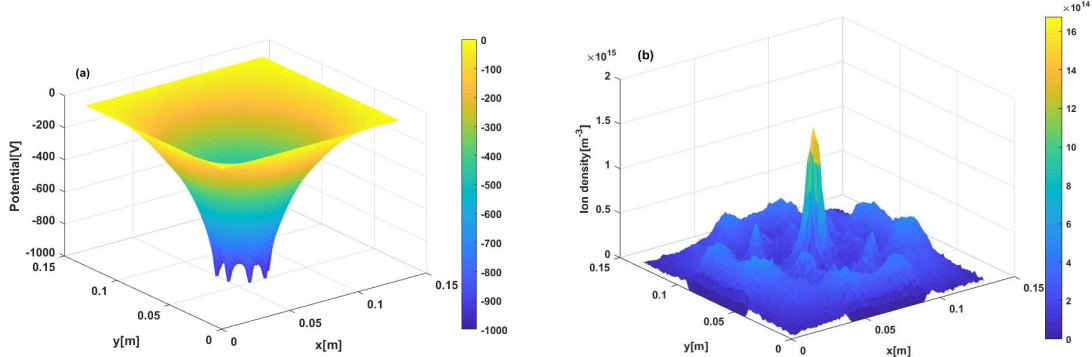


Figure 4: Surface plot of potential profile (a) and ion density profile (b) at  $-1\text{ kV}$  cathode voltage.

voltages are compared with the experimentally established graphs [30], as shown in figure(5). For lower cathode voltages, the ions re-circulate across the cathode openings until they collide with themselves or with the cathode grid. This results in scattering of the ions out of the potential trap. As the cathode voltage is increased, e.g. at  $-1\text{ kV}$ , the ion flux significantly increases inside the cathode, which results in the formation of a space charge of ions, i.e., a virtual anode inside the cathode (figure(5a)). Similar results are obtained during  $-2\text{ kV}$  and  $-3\text{ kV}$  cathode voltage operations, as shown in figures(5b) and (5c), respectively. The depth of the potential well is also found to be increasing with the increase in cathode voltage. The virtual anode formed causes further incoming ions to be reflected back before reaching it. However, the virtual anode serves as the potential trap for the secondary electrons (emitted from the gridded cathode due to the collision of ions) and they oscillate inside the virtual anode just like the ions in the outer trap. If the electron density increases, they in turn form a space charge of electrons which may lead to the formation of another virtual electrode, i.e., a virtual cathode inside the virtual anode. In principle, the process would continue to form multiple numbers of virtual electrodes inside the real cathode, but in practice, the potential trap formed by the secondary electrons, i.e., the first virtual cathode is all that is observed till date [1, 32]. The experimental results are in good agreement with the simulated results up to  $-3\text{ kV}$  cathode voltage, as shown in figure(5). The depth of the potential well increases as we increase the cathode potential and a prominent virtual anode at the center of the cathode grid have also been observed in the experimental plots. During  $-5\text{ kV}$  cathode voltage, a clear formation of a virtual cathode has been observed inside the cathode grid, experimentally [30], while in the simulated result (figure(6a)), only a slight indication of the virtual cathode is observed at the center. This is due to the limitations of the code specially during the simulation of higher voltage operations (around  $-5\text{ kV}$ ). The measurement of small potential variations inside the cathode is one of the difficult tasks in Particle-In-Cell method because of its statistical noise. The potential profiles presented here in this paper are the time averaged data (to overcome the fluctuation due to electron oscillation) of the specific configurations. For high voltage operation e.g.  $-5\text{ kV}$ , due to the additional trapping of electrons inside virtual anode, determining the accurate profile becomes more complicated.

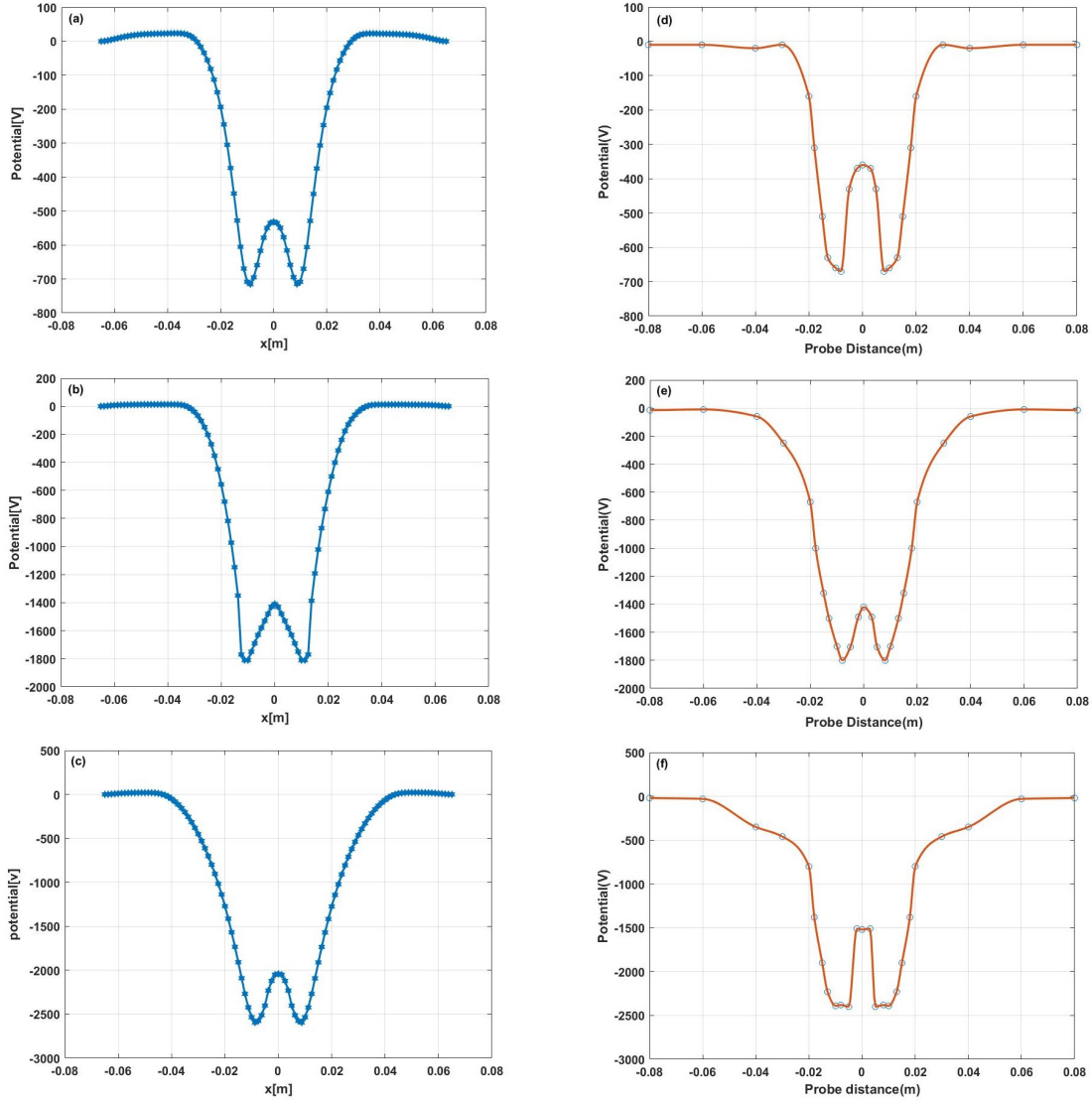


Figure 5: Potential profile in both simulated (a), (b) & (c) and experimental (d), (e) & (f) results during cathode voltage  $-1$ ,  $-2$  and  $-3$  kV, respectively.

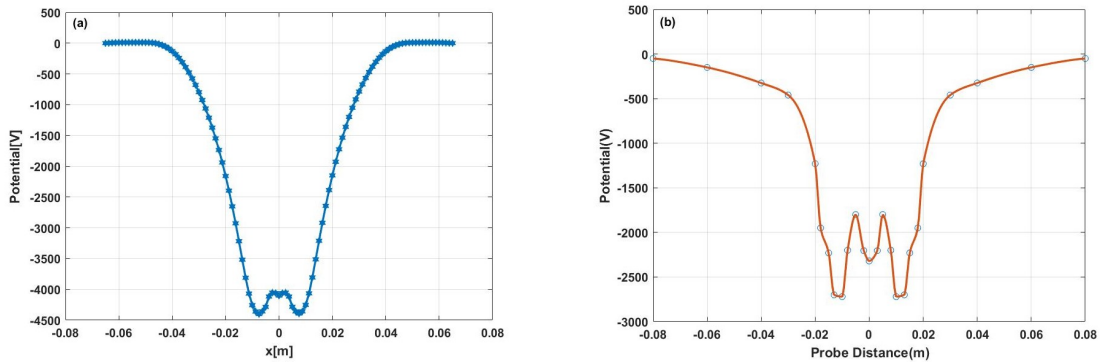


Figure 6: Potential profile in both simulated (a) and experimental (b) results during  $-5$  kV cathode voltage.

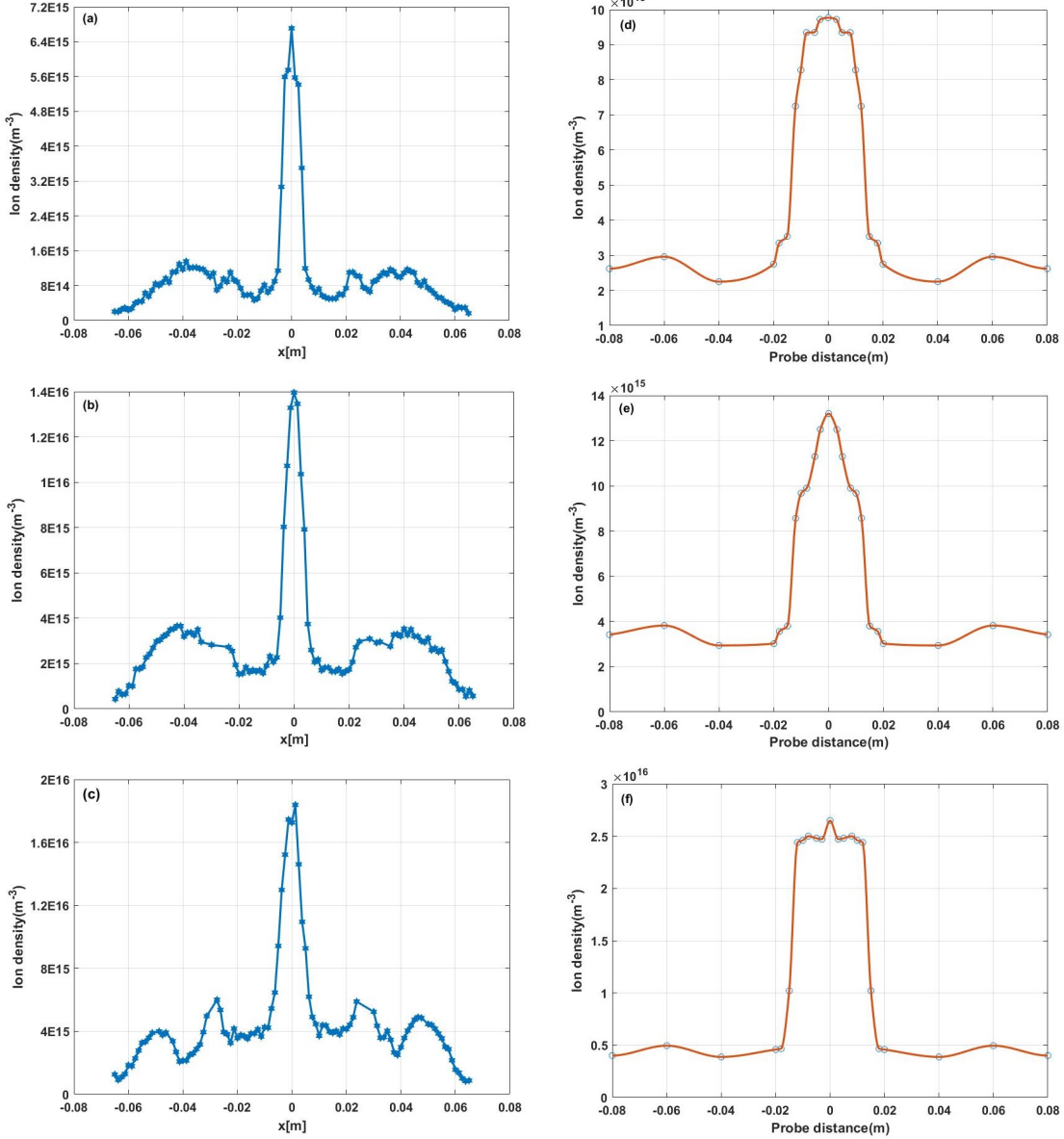


Figure 7: Ion density profile in both simulated (a), (b) & (c) and experimental (d), (e) & (f) results during  $-1$ ,  $-2$  and  $-3$  kV cathode voltage, respectively.

Therefore, in such cases, the signature of virtual anode formation as seen in figure(6a) is believed to be the proper justification of the detected profiles in the experiment (6b).

As already mentioned, ion density also plays a crucial role in the fusion reaction and to produce neutrons from such devices. We have studied the simulated ion density profiles up to a cathode voltage of  $-3$  kV and are shown in figure(7). An abrupt increase in ion density has been observed inside the cathode because of the trapped ions. At  $-1$  kV cathode voltage, the maximum density observed is  $6.8 \times 10^{15} m^{-3}$ , as shown in figure(7a). The density tends to be increasing as we gradually increase the cathode voltage, and at  $-3$  kV (figure(7c)) it is found to be one order higher ( $1.8 \times 10^{16} m^{-3}$ ) than the first case. In all the cases, ion

density outside the cathode, (near 0.04 m from the center) in both sides from the center, is observed to be slightly increasing. This is due to the re-circulating nature of the ions from one side to the other (figure(3a)). During the re-circulation process, the ions reaching the extreme position at one end achieve minimum velocity and turn back towards the negatively biased cathode with increased velocity. At the position of minimum velocity the density of ions must be higher in order to satisfy the ion continuity equation and to remain the ion flux conserved. A slight increase in ion density outside the cathode region is also observed in the experimental results. On the other hand, experimental results are showing similar kind of profiles, as depicted in figures(7d), (7e) and (7f) for cathode voltage  $-1$ ,  $-2$  and  $-3$  kV, respectively. Both the simulated and the experimental profiles indicate that the ion density at the core region increases with the applied cathode voltage and it is expected to be increasing further with higher cathode voltage.

#### 4.2. Ion energy distribution function (IEDF)

In order to measure the ion energy distribution from the simulation data, we have prepared a MATLAB script in which we can obtain IEDF profiles at different locations of the simulation domain [33, 34]. We have chosen three different locations, one inside and two outside the cathode grids, as shown in figure(8a), where IEDF's are measured during different cathode voltages. We have also chosen the x-component of velocity along which the IEDF is measured during three different cathode voltages,  $-1$ ,  $-2$  and  $-3$  kV, as shown in figure(8). Since the device is symmetrical along both x and y directions, the ions along y-component of velocity show similar type of characteristics as that of the ions along x-component. In case of  $-1$  kV cathode voltage, one peak is observed in the IEDF plots outside the cathode (1st zone) which suggests that only mono-energetic ions (primary ions due to ionization) are there in these positions. A second peak, in addition with the primary peak, is observed in the 2nd zone of the IEDF. The energy of the ions re-circulating across the cathode grids can be described by the second peak. Inside the cathode region (3rd zone), which is the area of interest, shows two distinct peaks at the tail of the distribution function along with the primary peak, as shown in figure(8b). The middle peak in the distribution function represents those ions which are re-circulating across the cathode from one side to the other with a particular set of energies. In this case, at the energy range of around 300 V, their distribution is maximum. Again, the ions which are trapped inside the potential well will have another particular range of energy (or frequency) than the ions outside the trap. These ions can be represented by the third peak (at around 650 V) at the high energy tail of the distribution function. Similar peaks are also observed at different energy ranges in case of  $-2$  and  $-3$  kV cathode voltage operations, as shown in figures(8c) and (8d), respectively. Another noticeable phenomenon that can be observed from the IEDF graphs is that the probability of re-circulation of the ions decreases as the cathode voltage increases from  $-1$  to  $-3$  kV. If we closely inspect the middle peak in the IEDF's measured inside the cathode region (3rd zone), it is found that the relative percentage of the area under the curve occupied by this peak gradually decreases with the increase in cathode voltage. In case of  $-1$  kV, the percentage of the area covered by the middle peak is

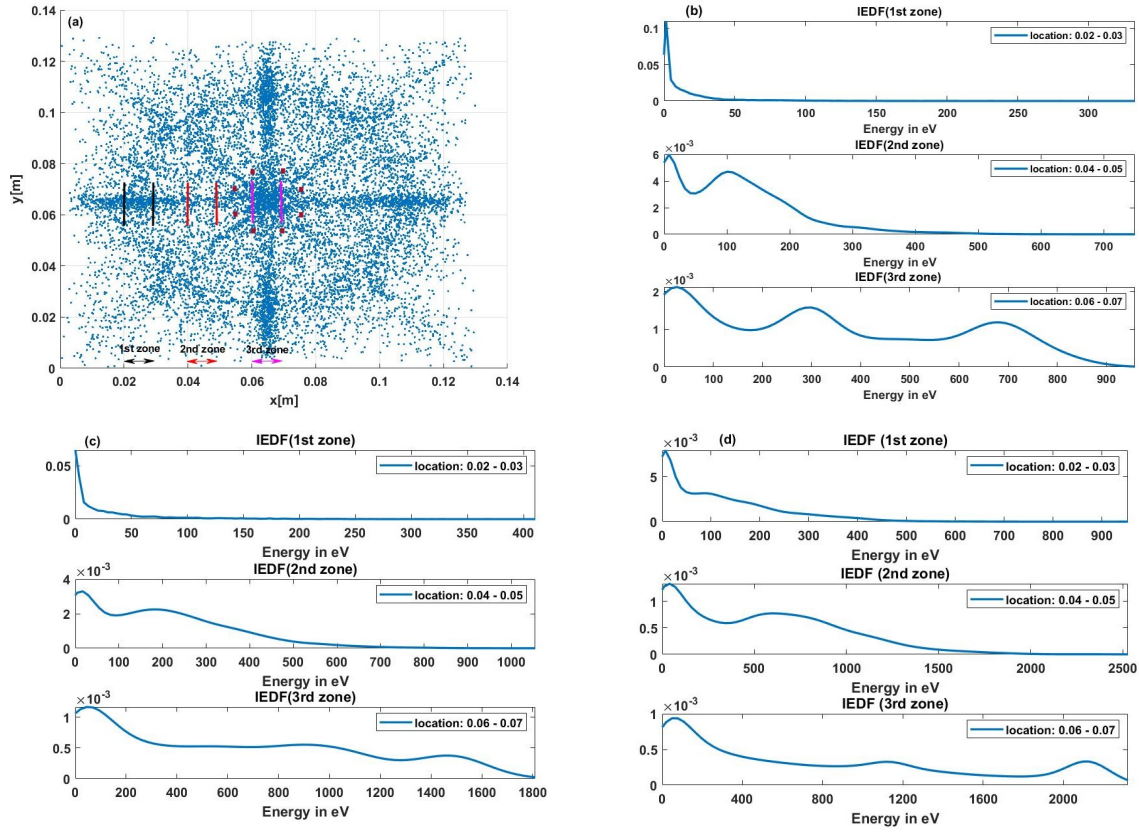


Figure 8: Different positions (zones) at which IEDF is measured is shown in figure (a). Simulated profiles of IEDF at cathode voltages  $-1$ ,  $-2$  &  $-3$  kV along x-component of velocity in three different zones are shown in figures(b), (c) & (d), respectively.

about 24% of the total area under the curve, while, it is declined to about 21% in the  $-2$  kV case. The relative area of the middle peak is further declined in  $-3$  kV case and it is found to be around 17% of the total area under the curve. On the contrary, the relative area covered by the third peak with respect to the second peak of the IEDF measured inside the cathode region, is found to be increasing with the increased cathode voltage. These results suggest that as the cathode voltage increases, the number of ions re-circulating across the cathode grids decreases, while the ions trapped inside the potential well increases.

## 5. Conclusion

The results obtained through simulation, in this paper, suggest that the potential profiles are in good agreement with the earlier obtained experimental profiles during applied cathode potential ranging from  $-1$  to  $-5$  kV. The depth of the potential well increases with the cathode voltage. An indication of the formation of multiple potential wells is also observed in the simulated profile during  $-5$  kV cathode voltage, while the experimental profile shows more prominent structure. Similarly, simulated profiles of ion density are also matching well with the experimental profiles. Lastly, the IEDF inside the cathode shows two peaks in

addition to the primary peak, which suggest that the ions at the center oscillate with different frequencies having a different sets of energies inside the potential well formed during high voltage operations. The second peak represents the ions which are re-circulating across the openings of the cathode grids and the last peak signifies the ions which are getting trapped at the core region. Moreover, it is observed that the percentage of re-circulating ions gradually decreases and simultaneously the trapped ions inside the potential well increases with the applied cathode voltage. As far as the future scopes are concerned, further upgradation of the code must be needed in order to perform the simulation during more higher voltage operations and to establish a concrete evidence of the formation of multiple potential wells inside the cathode.

The discharge process and the success of IECF device as a neutron source highly depend on the understanding of potential structure as well as on the ion dynamics inside the device. The present analyses are believed to serve as a reference guide to optimize technological parameters in IECF devices.

## Acknowledgments

The authors are grateful to the Director, Institute for Plasma Research (IPR), Gandhinagar, India and the Center Director, Center of Plasma Physics-Institute for Plasma Research (CPP-IPR), Sonapur, India, for providing us the opportunity to carry out this work. We are also thankful to Mr. M.K.D. Sarma for his technical support.

## References

- [1] Murali S K, Kulcinski G L, and Santarius J F. Study of ion flow dynamics in an inertial electrostatic confinement device through sequential grid construction. *Phys. Plasmas*, 15:122702, 2008.
- [2] Cipiti B B and Kulcinski G L. Embedded d-3he fusion reactions and medical isotope production in an inertial electrostatic confinement device. *Fusion Sci. Technol.*, 44(2):534, 2003.
- [3] Farnsworth P T. Electric discharge device for producing interactions between nuclei, June 28 1966. US Patent 3,258,402.
- [4] Hirsch R. Inertial-electrostatic confinement of ionized fusion gases. *J. Appl. Phys.*, 38:4522, 1967.
- [5] Nebel R A, Barnes D C, Caramana E J, Janssen R D, Nystrom W D, Tiouririne T N, Trent B C, Miley G H, and Javedani J. Inertial electrostatic confinement (iec) neutron sources. In *Proceedings of 16th International Symposium on Fusion Engineering*, volume 2, page 1229. IEEE, 1995.
- [6] Bussard R W and Krall N A. Inherent characteristics of fusion power systems: physics, engineering, and economics. *Fusion Technol.*, 26(4):1326, 1994.
- [7] Miley G H, Gu Y, DeMora J M, Stubbers R A, Hochberg T A, Nadler J H, and Anderl R A. Discharge characteristics of the spherical inertial electrostatic confinement (iec) device. *IEEE Trans. Plasma Sci.*, 25(4):733, 1997.
- [8] Dietrich C. *Improving particle confinement in inertial electrostatic fusion for spacecraft power and propulsion*. PhD thesis, Massachusetts Institute of Technology, 2007.
- [9] Takamatsu T, Masuda K, Kyunai T, Toku H, and Yoshikawa K. Inertial electrostatic confinement fusion device with an ion source using a magnetron discharge. *Nucl. Fusion*, 46(1):142, 2005.
- [10] Swanson D A, Cherrington B E, and Verdeyen Jo T. Potential well structure in an inertial electrostatic plasma confinement device. *Phys. Fluids*, 16(11):1939, 1973.

- [11] Thorson T A, Durst R D, Fonck R J, and Wainwright L P. Convergence, electrostatic potential, and density measurements in a spherically convergent ion focus. *Phys. Plasmas*, 4(1):4, 1997.
- [12] Thorson T A, Durst R D, Fonck R J, and Sontag A C. Fusion reactivity characterization of a spherically convergent ion focus. *Nucl. Fusion*, 38(4):495, 1998.
- [13] Yoshikawa K, Takiyama K, Yamamoto Y, Masuda K, Toku H, Koyama T, Taruya K, Hashimoto H, Ohnishi M, Horiike H, et al. Real time measurements of strongly localized potential profile through stark effects in the central core region of an inertial-electrostatic fusion device. In *18th IEEE/NPSS Symposium on Fusion Engineering. Symposium Proceedings (Cat. No. 99CH37050)*, page 27. IEEE, 1999.
- [14] Murali S K, Emmert G A, Santarius J F, and Kulcinski G L. Effects of chamber pressure variation on the grid temperature in an inertial electrostatic confinement device. *Phys. Plasmas*, 17(10):102701, 2010.
- [15] Miley G H, Wu L, and Kim J H. Nuclear techniques in national security studies on contraband detection. *J. Radioanal. Nucl. Chem.*, 263(1):159, 2005.
- [16] Cipiti B B and Kulcinski G L. Helium and deuterium implantation in tungsten at elevated temperatures. *J. Nucl. Mater.*, 347(3):298, 2005.
- [17] Boris D R. *Novel Diagnostic Approaches to Characterizing the Performance of the Wisconsin Inertial Electrostatic Confinement Plasma*. University of Wisconsin–Madison, 2009.
- [18] Noborio K, Yamamoto Y, Ueno Y, and Konishi S. Confinement of ions in an inertial electrostatic confinement fusion (iecf) device and its influence on neutron production rate. *Fusion Eng. Des.*, 81:1701, 2006.
- [19] Yamauchi K, Ogasawara K, Watanabe M, Okino A, Sunaga Y, and Hotta E. Neutron production characteristics and emission properties of spherically convergent beam fusion. *Fusion Technol.*, 39(3):1182, 2001.
- [20] Nevins W M. Can inertial electrostatic confinement work beyond the ion–ion collisional time scale? *Phys. Plasmas*, 2(10):3804, 1995.
- [21] Krall N A. The polywell<sup>TM</sup>: A spherically convergent ion focus concept. *Fusion Technol.*, 22(1):42, 1992.
- [22] Dolan T J. Magnetic electrostatic plasma confinement. *Plasma Phys. Control. Fusion*, 36(10):1539, 1994.
- [23] Ohnishi M, Sato K H, Yamamoto Y, and Yoshikawa K. Correlation between potential well structure and neutron production in inertial electrostatic confinement fusion. *Nucl. Fusion*, 37(5):611, 1997.
- [24] Ohnishi M, Osawa H, Yoshikawa K, Masuda K, and Yamamoto Y. Particle-in-cell simulation of inertial electrostatic confinement fusion plasma. *Fusion technol.*, 39(3):1211, 2001.
- [25] Buzarbaruah N, Dutta N J, Bhardwaz J K, and Mohanty S R. Design of a linear neutron source. *Fusion Eng. Des.*, 90:97, 2015.
- [26] Manura D, Dahl SIMION D, and SIMION Version. 8.0 user manual. scientific instrument services. Inc., NJ, 8551:28, 2016.
- [27] Buzarbaruah N, Dutta N J, Borgohain D, Mohanty S R, and Bailung H. Study on discharge plasma in a cylindrical inertial electrostatic confinement fusion device. *Phys. Lett. A*, 381(30):2391, 2017.
- [28] Buzarbaruah N, Mohanty S R, and Hotta E. A study on neutron emission from a cylindrical inertial electrostatic confinement device. *Nucl. Instrum. Methods Phys. Res.*, 911:66, 2018.
- [29] Verboncoeur J P, Langdon A B, and Gladd N T. An object-oriented electromagnetic pic code. *Comput. Phys. Commun.*, 87:199, 1995.
- [30] Bhattacharjee D, Jigdung D, Buzarbaruah N, Mohanty S R, and Bailung H. Studies on virtual electrode and ion sheath characteristics in a cylindrical inertial electrostatic confinement fusion device. *Phys. Plasmas*, 26(7):073514, 2019.
- [31] De Moura C A and Kubrusly S Carlos C S. The courant-friedrichs-lewy (cfl) condition. *Appl Math Comput*, 10:12, 2013.
- [32] Miley G H and Murali S K. *Inertial electrostatic confinement (IEC) fusion*. Springer, 2014.
- [33] Schwager L A and Birdsall C K. Collector and source sheaths of a finite ion temperature plasma. *Phys. Fluids B*, 2(5):1057, 1990.
- [34] Adhikari S, Moulick R, and Goswami K S. Ion dynamics in a magnetized source-collector sheath. *Phys. Plasmas*, 25(9):094504, 2018.